Accepted Article

This manuscript has been accepted after peer review and appears as an Accepted Article online prior to editing, proofing, and formal publication of the final Version of Record (VoR). This work is currently citable by using the Digital Object Identifier (DOI) given below. The VoR will be published online in Early View as soon as possible and may be different to this Accepted Article as a result of editing. Readers should obtain the VoR from the journal website shown below when it is published to ensure accuracy of information. The authors are responsible for the content of this Accepted Article.

COMMUNICATION

WILEY-VCH

Ping-pong intercomponent energy transfer in covalently linked porphyrin–MoS$_2$ architectures

Ruben Canton-Vitoria,[a]# Tobias Scharl,[b]# Anastasios Stergiou,[a] Alejandro Cadranel,[b, c, d] Raul Arenal,[e, f, g]* Dirk M. Guldi,[b]* Nikos Tagmatarchis[a]*

Abstract: Molybdenum disulfide nanosheets covalently modified with porphyrin were prepared and fully characterized. Neither the porphyrin absorption nor its fluorescence was notably impacted by covalent linkage to MoS$_2$. It was, however, with the help of transient absorption spectroscopy that a complex ping-pong energy transfer mechanism, namely from the porphyrin to MoS$_2$ and back to the porphyrin, was corroborated. This study reveals the potential of transition metal dichalcogenides in photosensitization processes.

Introduction

Molybdenum disulfide, MoS$_2$, is a typical example of layered transition metal dichalcogenides. In general, their structure is analogous to that of graphene, with an atomic layer of a transition metal sandwiched by two layers of chalcogen atoms. More specifically, each Mo atom is bound to six S atoms forming a three-atom thick monolayer.[1] Exfoliated MoS$_2$-materials have received enormous attention in recent years due to their extraordinary optoelectronic and electrocatalytic properties, especially in the area of energy applications and catalysis.[2, 3] Diverse exfoliation strategies have been developed for MoS$_2$. Most notable is the employment of (a) strong intercalants such as Li$^+$, which results in a phase transfer to an octahedral metallic 1T polytype,[4] and (b) non-oxidative Brønsted acids such as chlorosulfonic acid, which offers the benefit of retaining the 2H semiconducting phase.[5]

Nowadays additional efforts have been placed to develop strategies for chemically modifying transition metal dichalcogenides.[6] This is meant to fully harness the properties of, for example, MoS$_2$. In fact, incorporation of molecular dopants results in fine tuning of the electronic as well as optical properties of MoS$_2$ and, in turn, enables broadening the spectrum of its applications. In MoS$_2$, the S atoms in the basal plane are, however, rather inert due to saturation. Furthermore, Mo atoms are placed between S layers and, thereby challenging chemical reactivity. Still, covalent functionalization of MoS$_2$ has been accomplished.[7] For example, the basal plane of the 1T-MoS$_2$ polytype has been reacted with organoiodides,[8] while reaction with diazonium salts has been reported for the basal plane modification of 1T[9] as well as 2H-MoS$_2$.[10] In this work we adopt the recently developed methodology based on the addition of 1,2-dithiolanes on S-vacant sites located at the edges of exfoliated 2H-MoS$_2$ nanosheets.[11] In the context of the latter methodology, a true advantage is that diverse 1,2-dithiolanes are easily prepared and they react with exfoliated MoS$_2$ to yield interesting hybrids. Pyrene and phthalocyanines were, for example, interfaced with MoS$_2$.[11] Alternatively, ammonium moieties were grafted onto MoS$_2$ and WS$_2$, which facilitated the electrostatic association of carbon dots[12] and anionic porphyrins.[13] In the resulting ensembles, excited state intercomponent electronic interactions were responsible for the quenching of pyrene, carbon dots or porphyrin fluorescence. Major drawbacks of electrostatically associated ensembles are their lack of stability and of processing in organic solvents. They are also impacted by moderate bindings, especially when compared to the robust and strong bonding in covalently-linked conjugates. Therefore, it is not only imperative, but also timely, to explore the covalent modification of MoS$_2$ with photoactive porphyrins.

Herein, we report on the modification of the edges of exfoliated MoS$_2$ with a 1,2-dithiolane derivative **1**, featuring a porphyrin (H$_2$P). The newly prepared H$_2$P-MoS$_2$ **2** was comprehensively characterized by spectroscopic, thermal, and microscopy means. Beyond this characterization, we gathered insights into electronic interactions between the porphyrin and MoS$_2$ upon photoexcitation on the femto- to nanosecond timescales.

Results and Discussion

1,2-dithiolane-based porphyrin **1** was synthesized by a condensation reaction between α-lipoic acid and 5-(4-aminophenyl)-10,15,20-(triphenyl)porphyrin. In parallel, treatment of bulk MoS$_2$ with chlorosulfonic acid allowed the exfoliation of semiconducting nanosheets.[5] Next, reaction of

[a]   Dr. R. Canton-Vitoria, Dr. A. Stergiou, Prof. Dr. N. Tagmatarchis
        Theoretical and Physical Chemistry Institute
        National Hellenic Research Foundation
        48 Vassileos Constantinou Avenue, 11635 Athens, Greece.
        E-mail: tagmatar@eie.gr
[b]   Tobias Scharl, Dr. Alejandro Cadranel, Prof. Dr. Dirk M. Guldi
        Department of Chemistry and Pharmacy & interdisciplinary Center
        for Molecular Materials (ICMM), Friedrich-Alexander Universität
        Erlangen-Nürnberg
        Egerlandstr. 3, 91058 Erlangen, Germany.
        E-mail: dirk.guldi@fau.de
[c]   Dr. Alejandro Cadranel
        Universidad de Buenos Aires, Facultad de Ciencias Exactas y
        Naturales, Departamento de Química Inorgánica, Analítica y
        Química Física, Pabellón 2, Ciudad Universitaria, C1428EHA,
        Buenos Aires, Argentina.
[d]   Dr. Alejandro Cadranel
        CONICET – Universidad de Buenos Aires, Instituto de Química-
        Física de Materiales, Medio Ambiente y Energía (INQUIMAE),
        Pabellón 2, Ciudad Universitaria, C1428EHA Buenos Aires,
        Argentina.
[e]   Dr. Raul Arenal
        Laboratorio de Microscopias Avanzadas (LMA), Instituto de
        Nanociencia de Aragon (INA), U. Zaragoza, Mariano Esquillor s/n,
        50018 Zaragoza, Spain.
        E-mail: arenal@unizar.es
[f]   Dr. Raul Arenal
        Instituto de Ciencias de Materiales de Aragon, CSIC-U. de
        Zaragoza, Calle Pedro Cerbuna 12, 50009 Zaragoza, Spain.
[g]   Dr. Raul Arenal
        ARAID Foundation, 50018 Zaragoza, Spain.

[#]   Equal contribution

exfoliated MoS₂ with **1** yielded H₂P-MoS₂ **2**, as summarized in Figure 1. Filtration of the reaction mixture over a PTFE membrane (0.2 μm pore size) followed by extensive washing with dichloromethane, assured the removal of any non-covalently physisorbed **1** as revealed by UV-Vis spectroscopy (Figure S1). Purified **2** showed reasonable solubility in DMF, benzonitrile, and isopropanol, while it is completely insoluble in dichloromethane and water.
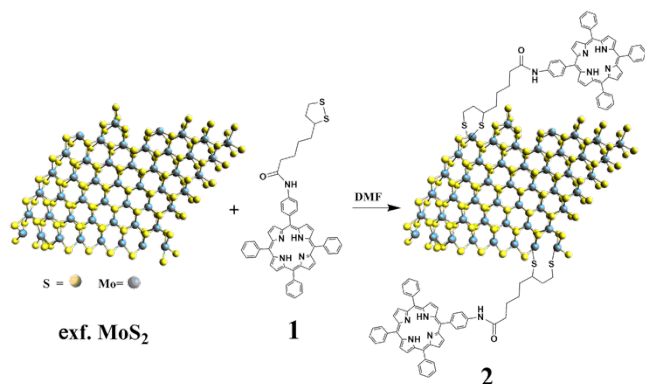

Figure 1. Reaction route for obtaining H₂P-MoS₂ **2**.

Evidence for the success in the covalent modification of MoS₂ with H₂P came from vibrational spectroscopy. Attenuated total reflectance infra-red ATR-IR measurements revealed for H₂P-MoS₂ **2** (Figure 2a) the presence of (a) C-H stretching vibration due to the alkyl chain, which connects H₂P with MoS₂, at 2848 and 2950 cm⁻¹, (b) amide carbonyl vibration at 1660 cm⁻¹, and (c) aromatic C=C bending at 1590 cm⁻¹. We further validated the origin of the IR bands related to H₂P within the hybrid by performing a blank experiment in which a mixture of tetraphenylporphyrin and exfoliated MoS₂ was processed under the same experimental conditions as those for obtaining **2**. The presence of physisorbed tetraphenylporphyrin was not detected in the UV-Vis and emission spectra of the blank material, while it did not show any contribution in the mass loss detected by TGA (Figure S2-S4).
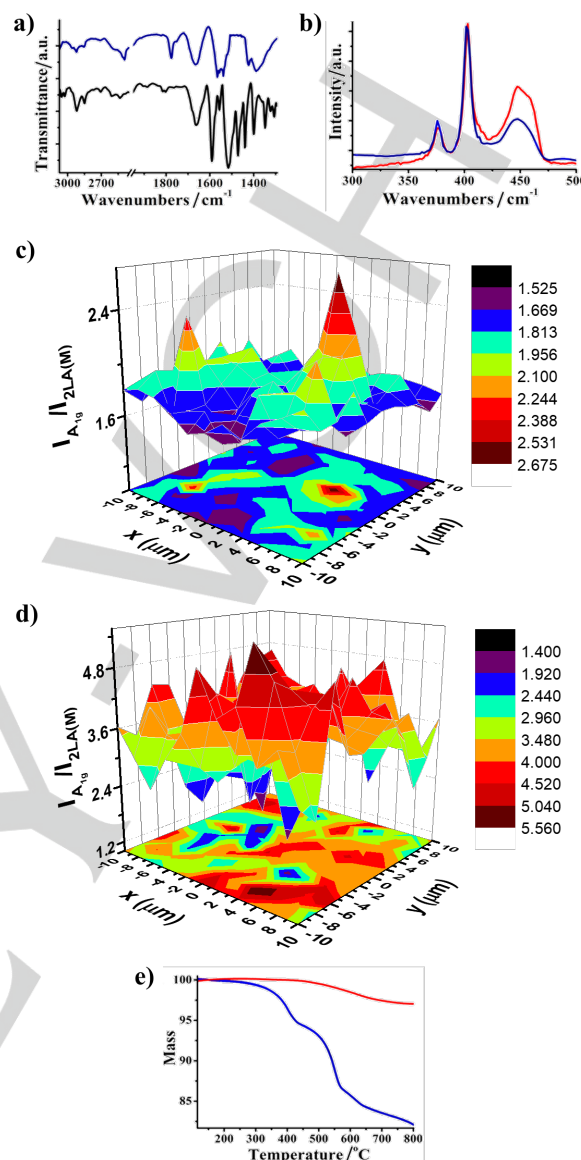

Figure 2. (a) ATR-IR spectra of **1** (black) and **2** (blue). (b) Raman spectra of exfoliated MoS₂ (red) and **2** (blue) upon excitation at 633 nm. (c, d) Raman mapping upon excitation at 633 nm of the I_A1g/I_2LA(M) intensity ratio of a 20μm x 20μm area for (c) exfoliated MoS₂, and (d) **2**. (e) TGA graphs of exfoliated MoS₂ (red) and **2** (blue).

Additional structural information regarding **2** came from Raman spectroscopy. Excitation at 514 nm brought the C=C and C=N bonds of H₂P to light in the 1000-1600 cm⁻¹ region (Figure S5). Focusing on the lower wavenumber region, characteristic modes due to MoS₂ were observed, especially upon excitation at 633 nm, due to coupling with the A1 excitonic transition, which in turn produces resonance Raman enhancement of the first and second order vibrational modes. Exfoliated semiconducting MoS₂ gave rise to: 2LA(M) at 447 cm⁻¹, A₁g at 406 cm⁻¹, and E¹₂g at 382 cm⁻¹ (Figure 2b). The difference frequency between A₁g and E¹₂g was found to be 24 cm⁻¹, from which we conclude the existence of few-layered MoS₂.[14, 15] Considering that the 2LA(M) vibration relates to the S-vacancies,[16] and comparing

WILEY-VCH

the Raman spectrum of exfoliated MoS_2 with that of **2**, the intensity ratio of A_{1g} over 2LA(M) was found to be considerably higher for **2**: i.e. 3.6 vs 1.9 for exfoliated MoS_2. Complementary Raman mapping assays revealed an increased $I_{A1g}/I_{2LA(M)}$ intensity ratio for **2** as compared to that for exfoliated MoS_2 (Figure 2c, d). This observation is in sharp contrast to the recorded $I_{A1g}/I_{2LA(M)}$ maps for the reference material prepared by physisorption (Figure S6). Overall, this is indicative of S-vacancies "healing" by the 1,2-dithiolane species in **2**.[9] Likewise, the absence of features at 150, 225, and 325 cm^{-1}, indicative of the metallic polytype, highlights the semiconducting nature of MoS_2 in **2**.

Thermogravimetric analysis (TGA) provided information related to the degree of MoS_2 functionalization in **2**. Exfoliated MoS_2 was found to be thermally stable under N_2 within 100-800°C. Notably, the mass loss observed in the modified MoS_2 is directly related to the thermal decomposition of the organic addends. Hence, the mass loss of 9% for **2** (Figure 2e) occurred up to 520°C is ascribed to the porphyrin. Based on this mass loss, a loading of one H_2P moiety per 54 units of MoS_2 was calculated. This is well in line with values reported for similar MoS_2 functionalization with pyrene and zinc phthalocyanine.[11]

Spatially-resolved electron energy loss spectroscopy (SR-EELS) using a scanning transmission electron microscope (STEM) enables investigating, at the local scale, the morphology and chemical composition of complex hybrid nanostructures.[17] Thus, we performed SR-EELS STEM analyses of **2**. Figure 3 displays an EEL spectrum-line (SPLI) recorded for a functionalized MoS_2 flake – see also Figure S7. Figure 3a corresponds to the high angular annular dark field (HAADF) STEM image of the flake and the SPLI was acquired following the highlighted green line. Typical EEL spectra are displayed in Figure 3b. Each of them corresponds to the sum of four EEL spectra extracted from the two areas marked in the SPLI (red (i) and green (ii) lines, respectively). $S-L_{2,3}$, $Mo-M_{4,5}$, C-K and $Mo-M_{2,3}$ edges are observed in both spectra. The energy loss near edge structure (ELNES) investigations of the C-K edge are displayed in the right panel of Figure S7. In the σ^* region (~290-325 eV), two signatures at 291.2 and 293.4 eV can be observed for **2**. Such signals are not discerned in the spectra recorded of other carbon containing materials employed as reference. Regarding the main contribution to the π^* signal at ~284-290 eV, we can also observe some differences. Here, the C-K edge is dominated by aromatic C contribution (~285.5 eV[17b-c, 18]), which in the case of H_2P is less pronounced. Furthermore, in the spectra recorded on **2**, another feature at ~287.2 eV is clearly seen. This signal can be attributed to pyrrolic (C-N) contributions of H_2P.[18c] Importantly, the N-K edge cannot be observed in H_2P due to the $Mo-M_{2,3}$ edge at the same energy range. For all these reasons, the features highlighted in the C-K edge of **2** correspond to porphyrin's contribution. Furthermore, we conclude from the EELS analyses that H_2P is homogenously distributed across the surface of the MoS_2 flakes in **2** (Figure S8).
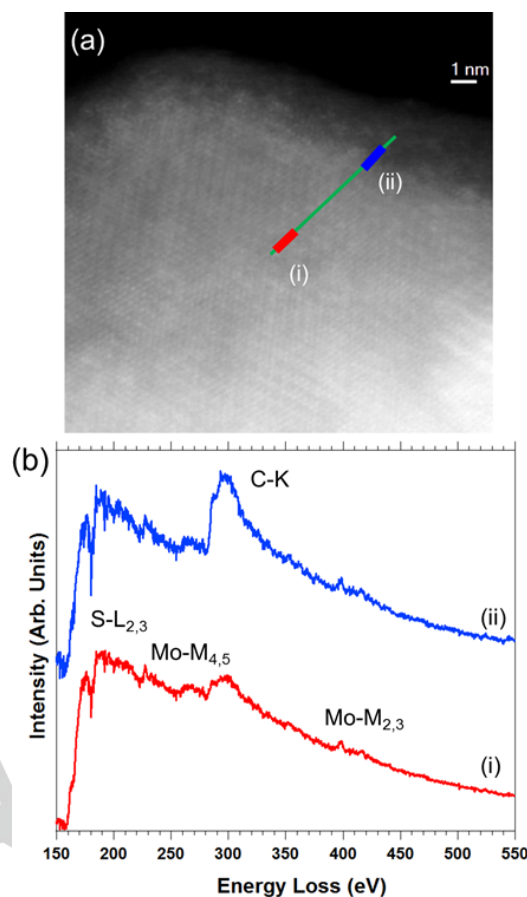

Figure 3. HAADF HRSTEM micrograph of a flake of **2**. An EELS SPLI has been acquired following the green marked line in this image. (b) Two EEL spectra, each of them corresponding to the sum of four selected EEL spectra collected from the two marked regions in the SPLI shown Fig. 3a. The $S-L_{2,3}$, $Mo-M_{4,5}$, C-K and $Mo-M_{2,3}$ edges are visible in both spectra. This detected carbon is associated to H_2P.

Next, focusing on the optical properties of **2**, the UV-Vis spectrum was registered in DMF and compared with that of **1**. In particular, the UV-Vis of **1** showed a sharp absorption at 418 nm due to the Soret band, accompanied by weaker Q-band absorptions at 516, 550, 596, and 648 nm (Figure 4a). In the UV-Vis of exfoliated MoS_2, spectroscopic fingerprints are discernable at 401, 494 (C-exciton), 626 (B-exciton), and 681(A-exciton) nm (Figure 4a). The UV-Vis of **2** is best described as superimposition of the individual spectra, namely **1** and exfoliated MoS_2. The spectrum is, for example, dominated by the characteristic Soret-band absorption of H_2P at 418 nm in addition to the MoS_2 related transition at 679 nm. From their similarity we deduce that the ground-state lacks appreciable electronic interactions.

Excited-state electronic interactions also appeared suitable to probe interactions between H_2P and MoS_2 in **2**. Specifically, upon excitation at the Soret-band absorption at 420 nm, strong fluorescence, which was centered at 651 and 715 nm (Figure 4b), was found for **1**. In TCSPC measurements, a fluorescent lifetime of 10.3 ns (Figure S9) was determined for **1** with DMF as

solvent. 420 nm photoexcitation of **2** resulted, however, in no significant quenching of the porphyrin centered fluorescence relative to that of **1** (Figure 4b). For **2**, the fluorescence maxima were observed at 649 and 714 nm, and the fluorescence lifetime was 10.3 ns (Figure S9).
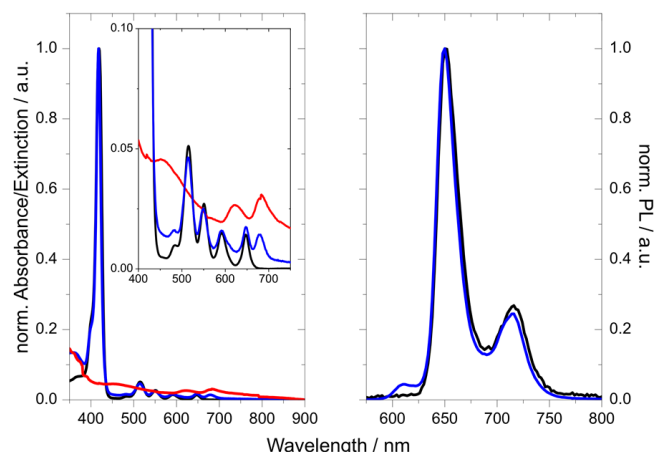

Figure 4. (a) Electronic absorption spectra of **1** (black), exfoliated MoS_2 (red), and **2** (blue) in DMF. (b) Fluorescence spectra of **1** (black) and **2** (blue) in DMF upon excitation at 420 nm.

As a complement to the aforementioned, we probed **1**, exfoliated MoS_2, and **2** by means of femtosecond transient absorption spectroscopy (fsTAS) using 420 nm as excitation wavelength (Figures S10 and S11, and Figure 5, respectively). For **1**, ground-state bleaching at 517 and 653 nm are observed early on in the experiments. In addition, positive absorptions evolved at 442, 538, 574, 623, and 690 nm (Figure S10). Global analysis revealed on the fsTAS timescale the presence of three exponential decays. These three decays are followed by a much slower decay, whose dynamics are outside of the timescale of our experiments. Therefore, a target model was applied to fit the transient absorption data (Figure 6, right). It involves an initial population of second singlet excited state (S_2), consistent with excitation into the Soret-band absorption, which internally converts to first singlet excited state (S_1) in 16 ps. The latter intersystem crosses in 10 ns to the triplet manifold (T_1), which, in turn, decays back to the ground state on the microsecond timescale. Additionally, aggregates of **1** are present in the sample and they were found to decay to the ground state in 142 ps. These dynamics resemble very closely those already reported for a variety of porphyrins.[19, 20]
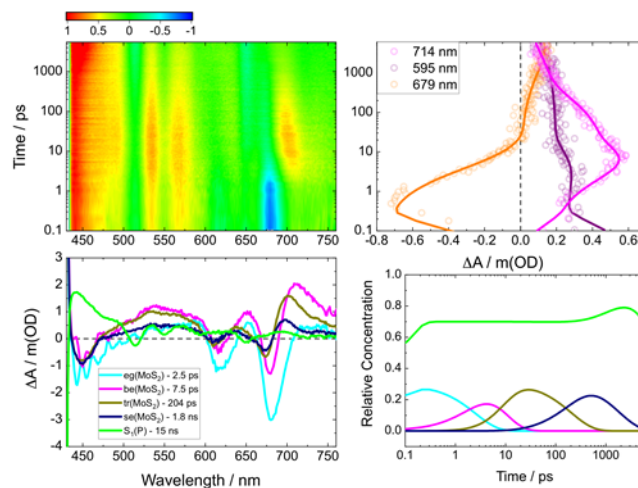

Figure 5. Upper left: Differential absorption 3D map obtained upon fsTAS of **2** in DMF at room temperature with 420 nm excitation. Upper right: Time absorption profiles and fits at selected wavelengths. Bottom left: Species associated differential spectra of exciton generation (eg – cyan curve), biexcitons (be – pink curve), trions (tr – brown curve), single excitons (se – dark blue curve) and singlet excited state (S_1 – green curve). Bottom right: Concentration evolution of the different species over time.

For exfoliated MoS_2, ground-state bleaching evolved at 476, 623, and 683 nm together with positive absorptions at 591, 655, and 743 nm (Figure S11). Global analysis of the data revealed five exponential decays that follow light absorption. The first three species, which take place with 2.7, 7.3 and 250 ps, involve biexciton (be) and trion (tr) formation as well as the decay of these many-body particles, respectively, into single excitons (se). Single excitons then diffuse in 1.8 ns across the layers in the z direction (de), before they recombine to recover the ground state in 21.2 ns (Figure 6, left). These dynamics resemble those already reported for exfoliated MoS_2.[21]

For **2**, excited states of both components are observed to participate in the decay cascade (Figure 5). Selective excitation into the Soret-band absorption of **2** affords a photoinduced absorption at 450 nm and ground-state bleaching at 617 and 679 nm. Please note that, while the first belongs to the porphyrin, the last two are fingerprints of MoS_2. Considering that, at the excitation wavelength, porphyrin absorptions in **2** are around 20 times stronger than those of MoS_2 (Figure 4a), the similar intensities of the differential features at 450 and 679 nm imply an ultrafast energy transfer (<1 ps) from S_2, which is populated upon 420 nm excitation, to MoS_2. Upon global analysis, we noted four exponential decays on the fsTAS timescale and an additional decay, which is, however, outside of our detection range. Our interpretation is based on a kinetic target model, which is depicted in the middle panel of Figure 6. It considers an initial excited state population governed by a porphyrin-centered S_2, with a minority of a MoS_2-centered excited state. This is followed by a non-quantitative ultrafast energy transfer from H_2P to MoS_2, which results in comparable populations of H_2P-centered (70%) and MoS_2-centered (30%) excited states. Afterwards, the same three species, which govern the deactivation of exfoliated MoS_2, and, which result in the

formation of single excitons, are discernible. The times that it takes to interconvert are 2.5, 7.5 and 204 ps, respectively. Once populated, the single exciton of MoS_2 is subject to a second energy transfer. This time it is, however, from the single excitons of MoS_2 to the S_1 of H_2P. This energy transfer takes 1.75 ns. From here, the porphyrin decay proceeds via intersystem crossing to the corresponding triplet excited state in 14 ns, and ground state recovery on the microsecond timescale. This mechanism is also based on the energetics of **2**. The S_1 of **1** with its fluorescence at 1.73 eV (715 nm) and the MoS_2 fluorescence at 1.82 eV[22] render the second energy transfer a downhill process. With the ping-pong energy transfer model we rationalize the nearly identical steady-state photophysical characteristics of **1** and **2** upon photoexcitation.

Figure 6. Deactivation models for MoS_2 (left), **2** (middle) and **1** (right) upon 420 nm excitation.

Conclusion

In summary, we accomplished the covalent grafting of porphyrin **1** onto exfoliated MoS_2, forming novel H_2P-MoS_2 **2**, which was fully characterized. Full-fledged photophysical investigations based on steady-state and time-resolved measurements corroborate that the decay of the photoexcited porphyrin involves a ping-pong energy transfer to and from MoS_2. Our findings suggest that transition metal dichalcogenides have great potential in photosensitization. Such hybrid materials may be useful in energy conversion applications.

Acknowledgements

MoS_2 • porphyrin • 1,2-dithiolane • hybrid • sensitizers

[1]   a) X. Huang, Z. Zeng, H. Zhang, *Chem. Soc. Rev*. **2013**, *42*, 1934; b) M. Xu, T. Liang, M. Shi, H. Chen, *Chem. Rev*. **2013**, *113*, 3766; c) R. Lv, J. A. Robinson, R. E. Schaak, D. Sun, Y. Sun, T. E. Mallouk, M. Terrones, *Acc. Chem. Res*. **2015**, *48*, 56.

[2]   a) D. Jariwala, V. K. Sangwan, L. J. Lauhon, T. J. Marks, M. C. Hersam, *ACS Nano*, **2014**, *8*, 1102; b) A. Pospischil, M. M. Furchi, T. Mueller, *Nat. Nanotechnol*. **2014**, *9*, 257; c) M. Pumera, Z. Sofer, A. Ambrosi, *J. Mater. Chem. A*, **2014**, *2*, 8981; d) T. Stephenson, Z. Li, B. Olsen, D. Mitlin, *Energy Environ. Sci*. **2014**, *7*, 209; e) X. Zhang, L. Hou, A. Ciesielski, P. Samori, *Adv. Energy Mater. 2016*, *6*, 1600671; f) X. Zhang, Z. Lai, C. Tan, H. Zhang, *Angew. Chem. Int. Ed*. **2016**, *55*, 8816

[3]   a) D. Voiry, H. Yamaguchi, J. Li, R. Silva, D. C. B. Alves, T. Fujita, M. Chen, T. Asefa, V. B. Shenoy, G. Eda, M. Chhowalla, *Nat. Mater*. **2013**, *12*, 850; b) A. Y. S. Eng, A. Ambrosi, Z. Sofer, P. Simek, M. Pumera, *ACS Nano*, **2014**, *8*, 12185; c) X. Chia, A. Y. S. Eng, A. Ambrosi, S. M. Tan, M. Pumera, *Chem. Rev*. **2015**, 115, 11941; d) S. J. Rowley-Neale, C. W. Foster, G. C. Smith, D. A. C. Brownson, C. E. Banks, *Sustainable Energy Fuels,* **2017**, 1, 74; e) D. K. Perivoliotis, N. Tagmatarchis, *Carbon* **2017**, *118*, 493.

[4]   a) J. Zheng, H. Zhang, S. Dong, Y. Liu, C. T. Nai, H. S. Shin, H. Y. Jeong, B. Liu, K. P. Loh, *Nature Commun*. **2014**, *5*, 2995; (b) Y. Yao, L. Tolentino, Z. Yang, X. Song, W. Zhang, Y. Chen, C.-P. Wong, *Adv. Funct. Mater*. **2013**, *23*, 3577; c) G. Eda, H. Yamaguchi, D. Voiry, T. Fujita, M. Chen, M. Chhowalla, *Nano Lett*. **2011**, *11*, 5111; d) Z. Tang, Q. Wei, B. Guo, *Chem. Commun*. **2014**, *50*, 3934.

[5]   G. Pagona, C. Bittencourt, R. Arenal, N. Tagmatarchis, *Chem. Commun*. **2015**, *51*, 12950.

[6]   a) M. Chhowalla, H. S. Shin, G. Eda, L. -J. Li, K. P. Loh, H. Zhang, *Nat. Chem*. **2013**, *5*, 2635; (b) X. Chen, A. R. McDonald, *Adv. Mater*. **2016**, *28*, 5738.

[7]   a) E. Grayfer, M. Kozlova, V. Fedorov, *Adv. Colloid Interface Sci*. **2017***, 245*, 40*;* b) A. Stergiou, N. Tagmatarchis, *Chem. Eur. J*. **2018***, 24*, 18246; c) S. Bertolazzi, M. Gobbi, Y. Zhao, C. Backes, P. Samori, *Chem. Soc. Rev*. **2018***, 47*, 6845.

[8]   D. Voiry, A. Goswami, R. Kappera, C. C. Silva, D. Kaplan, T. Fujita, M. Chen, T. Asefa, M. Chhowalla, *Nature Chem*. **2015**, *7*, 45.

[9]   a) K. C. Knirsch, N. C. Berner, H. C. Nerl, C. S. Cucinotta, Z. Gholamvand, E. McEvoy, Z. Wang, Abramovic, I. P. Vecera, M. Halik, S. Sanvito, G. S. Duesberg, V. Nicolosi, F. Hauke, A. Hirsch, J. N. Coleman, C. Backes, *ACS Nano* **2015**, *9*, 6018; b) E. E. Benson, H. Zhang, S. A. Schuman, S. U. Nanayakkara, N. D. Bronstein, S. Ferrere, J. L. Blackburn, E. M. Miller, *J. Am. Chem. Soc*. **2018**, *140*, 441.

[10]   X. Chu, A. Yousaf, D. Li, A. Tang, A. Debnath, D. Ma, A. Green, E. Santos, Q. Wang, *Chem. Mater*. **2018**, *30*, 2112.

[11]   a) R. Canton-Vitoria, Y. Sayed-Ahmad-Baraza, M. Pelaez-Fernandez, R. Arenal, C. Bittencourt, C. P. Ewels, N. Tagmatarchis, *NPJ 2D Mater. Appl*. **2017**, *1*, 13; b) R. Canton‐Vitoria, H. B. Gobeze, V. M. Blas‐Ferrando, J. Ortiz, Y. Jang, F. Fernández‐Lázaro, Á. Sastre‐Santos, Y. Nakanishi, H. Shinohara, F. D'Souza, N. Tagmatarchis *Angew. Chem. Int. Ed*. **2019**, *58*, 5712.

[12]   R. Canton-Vitoria, L. Vallan, E. Urriolabeitia, A. M. Benito, W. K. Maser, N. Tagmatarchis, *Chem. Eur. J*. **2018***, 24*, 10468.

[13]   R. Canton-Vitoria, C. Stangel, N. Tagmatarchis, *ACS Appl. Mater. Interfaces* **2018**, *10*, 23476.

[14]   M. A. Pimenta, E. Corro, B. R. Carvalho, C. Fantini, L. M. Malard, *Acc. Chem. Res*. **2015**, *48*, 41.

[15]   a) H. Li, Q. Zhang, C. C. R. Yap, B. K. Tay, T. H. T. Edwin, A. Olivier, D. Baillargeat, *Adv. Funct. Mater*. **2012**, *22*, 1385; b) S.-L. Li, H. Miyazaki, H. Song, H. Kuramochi, S. Nakaharai, K. Tsukagoshi, *ACS Nano* **2012**, *6*, 7381.

[16]   S. Bae, N. Sugiyama, T. Matsuo, H. Raebiger, K.-i. Shudo, K. Ohno, *Phys. Rev. Appl*. **2017**, *7*, 024001.

COMMUNICATION

[17] a) R. Arenal, F. de la Pena, O. Stephan, M. Walls, A. Loiseau, C. Colliex, *Ultramicroscopy*, **2018**, *109*, 32; b) A. Setaro, M. Adeli, M. Glaeske, D. Przyrembel, T. Bisswanger, G. Gordeev, F. Maschietto, A. Faghani, B. Paulus, M. Weinelt, R. Arenal, R. Haag, S. Reich, *Nat. Commun.* **2017**, *8*, 14281; c) R. Arenal, L. De Matteis, L. Custardoy, A. Mayoral, M. Tence, V. Grazu, J. M. De La Fuente, C. Marquina, M. R. Ibarra, *ACS Nano* **2013**, *7*, 4006.

[18] a) S. Dubey, S. Lisi, G. Nayak, F. Herziger, V. D. N'Guyen, T. Le Quang, V. Cherkez, C. González, Y. Dappe, K. Watanabe, T. Taniguchi, L. Magaud, P. Mallet, J.Y. Veuillen, R. Arenal, L. Marty, J. Renard, N. Bendiab, J. Coraux, V. Bouchiat, *ACS Nano* **2017**, *11*, 11206; b) A. Setaro, M. Adeli, M. Glaeske, D. Przyrembel, T. Bisswanger, G. Gordeev, F. Maschietto, A. Faghani, B. Paulus, M. Weinelt, R. Arenal, R. Haag, S. Reich, *Nat. Commun.* **2017**, *8*, 14281; c) R. Arenal, K. March, C.P. Ewels, X. Rocquefelte, M. Kociak, A. Loiseau, O. Stephan, Nano Lett. 2014, 14, 5509; d) R. Arenal, A. Lopez-Bezanilla, *ACS Nano* **2014**, *8*, 8419.

[19] A. Cadranel, V. Strauss, J. T. Margraff, K. A. Winterfeld, C. Vogl, L. Dordevic, F. Arcudi, H. Hoelzel, N. Jux, M. Prato, D. M. Guldi, *J. Am. Chem. Soc.* **2018**, *140*, 904.

[20] T. Scharl, A. Cadranel, P. Haines, V. Strauss, S. Bernhardt, S. Vela, C. Atienza, F. Gröhn, N. Martín, D. M. Guldi, *Chem. Comm.* **2018**, *54*, 11642.

[21] L. Wibmer, S. Lages, T. Unruh, D. M. Guldi, *Adv. Mater.* **2018**, *30*, 1706702.

[22] S. Padgaonkar, S. H. Amsterdam, H. Bergeron, K. Su, T. J. Marks, M. C. Hersam, E. A. Weiss, *J. Phys. Chem. C* **2019**,*123*, 13337.

COMMUNICATION

Entry for the Table of Contents

COMMUNICATION

Complex ping-pong energy transfer, from porphyrin to MoS_2 and back to porphyrin, was corroborated in a porphyrin-MoS_2 hybrid material.
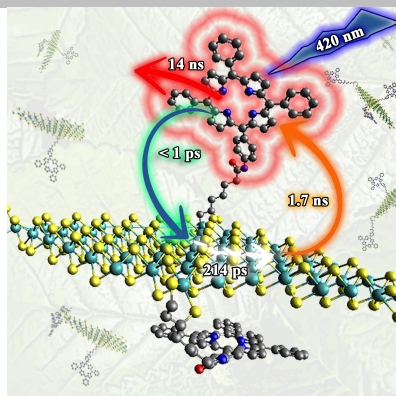
Ruben Canton-Vitoria, Tobias Scharl, Anastasios Stergiou, Alejandro Cadranel, Raul Arenal,* Dirk M. Guldi,* Nikos Tagmatarchis*